
5

Prediction of human CNS pharmacokinetics using a physiologically based pharmacokinetic modeling approach

Y Yamamoto, P A Välitalo, Y C Wong, D R Huntjens, J H Proost, A Vermeulen, W Krauwinkel, M W Beukers, H Kokki, M Kokki, M Danhof, J G C van Hasselt, E C M de Lange

Submitted for publication

ABSTRACT

Knowledge of drug concentration-time profiles at the central nervous system (CNS) target-site is critically important for rational development of CNS targeted drugs. Our aim was to translate a recently published comprehensive CNS physiologically based pharmacokinetic (PBPK) model from rat to human, and to predict drug concentration-time profiles in multiple CNS compartments on available human data of four drugs (acetaminophen, oxycodone, morphine and phenytoin).

Values of the system-specific parameters in the rat CNS PBPK model were replaced by corresponding human values. The contribution of active transporters for the four selected drugs was scaled based on differences in expression of the pertinent transporters in both species. Model predictions were evaluated with available pharmacokinetic (PK) data in human brain extracellular fluid and/or cerebrospinal fluid, obtained under physiologically healthy CNS conditions (acetaminophen, oxycodone, and morphine) and under pathophysiological CNS conditions where CNS physiology could be affected (acetaminophen, morphine and phenytoin).

The human CNS PBPK model could successfully predict their concentration-time profiles in multiple human CNS compartments in physiological CNS conditions within a 1.6-fold error. Furthermore, the model allowed investigation of the potential underlying mechanisms that can explain differences in CNS PK associated with pathophysiological changes. This analysis supports the relevance of the developed model to allow more effective selection of CNS drug candidates since it enables the prediction of CNS target-site concentrations in humans, which are essential for drug development and patient treatment.

INTRODUCTION

Development of drugs for central nervous system (CNS) diseases faces high attrition rates (1). A major factor for this high attrition rate is the lack of adequate information on unbound drug concentration-time profile at the CNS target-sites, which is the driving force for the drug-target interaction and subsequent drug effect (2).

Several factors govern the distribution of drug molecules into and within the CNS. Physiological CNS compartments include the brain microvascular space, the key drug-target site compartments being the brain extracellular fluid ($brain_{ECF}$), the brain intracellular fluid ($brain_{ICF}$), and also multiple cerebrospinal fluid (CSF) spaces. CNS drug distribution is governed by several processes including physiological fluid flows, passive and active membrane transport across the blood–brain barrier (BBB) and the blood–CSF barrier (BCSFB), extracellular-intracellular exchange, and pH differences (3). Physiological fluid flows include cerebral blood flow (CBF), $brain_{ECF}$ bulk flow, and CSF flow. The interplay between various processes complicates prediction of drug target-site concentrations. In addition, aging and pathophysiological conditions may alter CNS drug distribution. This happens for example via changes in properties of the BBB and BCSFB (e.g. tight junctions, active transporters), volumes of CNS compartments and CNS fluid flows (4,5), and should therefore be taken into account in CNS pharmacokinetics (PK) predictions.

To investigate CNS drug distribution, *ex vivo* techniques such as the brain homogenate and the brain slicing technique are currently used. With these techniques, steady state values of the unbound fraction in brain (6) and the volume of distribution of the unbound drug in brain (7) can be determined, from which also intracellular accumulation of the unbound drug can be derived. Unfortunately, these techniques cannot provide information on the unbound drug concentration-time profiles, and potential local concentration differences. Such information is very important for determining the rate and extent of processes in CNS drug distribution and understanding their interrelationships (systems pharmacokinetics). Time course data of unbound drug concentrations can only be obtained by *in vivo* intracerebral microdialysis (8–11), as other monitoring techniques like positron emission tomography measure total drug concentrations (12–14). However, though minimally invasive, the use of microdialysis in humans is highly restricted. Therefore, approaches that can predict time-dependent and CNS location-dependent unbound drug concentration in human are of great interest.

We recently developed a comprehensive physiologically based pharmacokinetic (PBPK) rat model to predict unbound drug concentration-time profiles for multiple CNS compartments (15). This rat PBPK model allows prediction of CNS PK profiles without the need of *in vivo* PK data. The purpose of the present study was to scale the rat CNS PBPK model to predict drug PK profiles in multiple CNS compartments in human. The human CNS PBPK model was evaluated using available human $brain_{ECF}$ and/or CSF PK data in physiological and/or pathophysiological CNS conditions, on acetaminophen, oxycodone, morphine, and phenytoin.

MATERIALS AND METHODS

The previously developed rat CNS PBPK model (15), which consisted of a plasma PK and a CNS PBPK component, was scaled to predict human CNS PK by substitution of rat CNS physiological parameter values by the human values (**Figure 1**). Human plasma PK models for the drugs investigated (acetaminophen, oxycodone, morphine, phenytoin) were either obtained from literature or developed using available human plasma data.

All analyses were performed using NONMEM version 7.3 (16). The predictive performance of the developed model was evaluated using available human data on the concentrations of acetaminophen, oxycodone, morphine and phenytoin in $brain_{ECF}$ and/or CSF, obtained under physiological and/or pathophysiological CNS conditions.

Human plasma and CNS data

The details of the clinical PK studies of acetaminophen, oxycodone, morphine and phenytoin, which were used for the evaluation of the human PBPK model predictions, are summarized in **Table I**.

Acetaminophen

Human acetaminophen PK data in plasma and in CSF in the lumbar region (CSF_{SAS_LUMBAR}) were obtained from healthy subjects (study A1) and from patients with nerve-root compression pain (study A2) (17,18). These CNS conditions were considered to be physiological CNS conditions, i.e. without likely effects on CNS PK. In study A3, human CSF samples from the lateral ventricle (CSF_{LV}) were obtained by extra-ventricular drainage (EVD) (CSF_{EVD}) from patients with traumatic brain injury (TBI), which was considered to be a pathophysiological CNS condition (19). For all datasets, total plasma concentrations for acetaminophen were converted to unbound plasma concentrations using the free fraction (85%) obtained from literature for healthy subjects (20).

Oxycodone

Oxycodone human plasma and CSF_{SAS_LUMBAR} PK data (study O1) were obtained from patients under elective gynecological surgery (21), where a CNS condition considered to be physiological. Unbound plasma concentrations for oxycodone were extrapolated from the total plasma concentrations using the free fraction (59%) obtained from literature for healthy subjects (22,23).

Morphine

Morphine human PK data in plasma and in $brain_{ECF}$ (study M1 and M2) were obtained from bilateral microdialysis measurements from both the injured and uninjured brain sides of TBI patients, thereby providing a comparison of physiological and pathophysiological conditions (24,25). For both datasets, the unbound plasma concentrations were reported in these original publications.

Phenytoin

Phenytoin human PK data in plasma and in CSF_{SAS_LUMBAR} (study P1) were obtained from epileptic patients, which was considered a pathophysiological CNS condition (26). Unbound plasma concentrations for phenytoin were extrapolated from the total plasma concentrations using the free fraction (13%) obtained from literature for healthy subjects (27).

Human plasma PK models

For acetaminophen (study A3) and morphine (study M1 and M2), we used published human plasma PK models (19). For acetaminophen (study A1 and A2), oxycodone (study O1) and phenytoin (study P1), plasma PK models were systematically developed with a mixed effects modeling approach using available individual human plasma data, since there is no plasma PK model from literature or the existing plasma PK model did not adequately describe the data (19) (see Table I). One-, two- and three-compartment models were evaluated for their utility to describe the data. Inter-individual variability was incorporated on each PK parameter, using an exponential model. Proportional and combined additive-proportional residual error models were tested. Model selection was guided by a likelihood ratio test with $p<0.05$, the precision of the parameter estimates, assessment of the parameter correlation matrix, and graphical evaluation of the plots for observations *versus* predictions, weighted residuals *versus* time, and weighted residuals *versus* predictions (28).

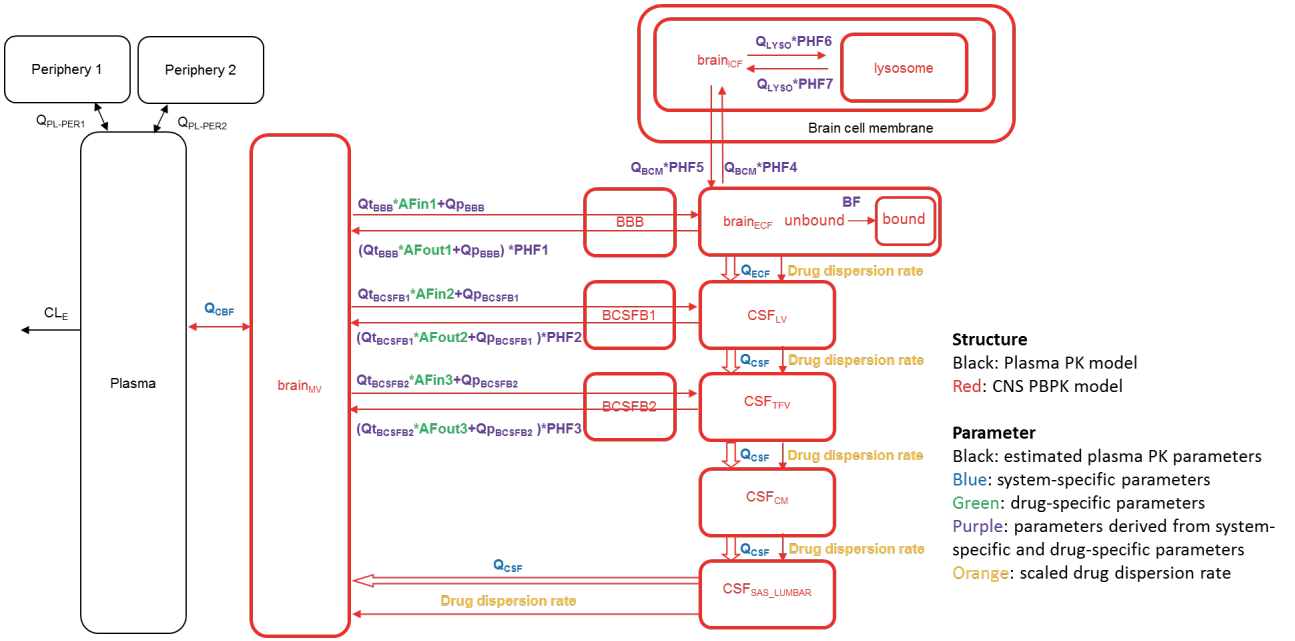

Figure 1. The human PBPK model structure.
The model consists of a plasma PK model and a CNS PBPK model with estimated plasma PK parameters, and system-specific and drug-specific parameters (colors) for CNS. The plasma PK model was extended with peripheral compartments 1 and 2 in cases where these compartments were required to describe the plasma data adequately. $Brain_{MV}$: brain microvascular, BBB: blood-brain barrier, BCSFB: blood-CSF barrier, $brain_{ECF}$: brain extra cellular fluid, $brain_{ICF}$: brain intra cellular fluid, CSF_{LV}: CSF in the lateral ventricle, CSF_{TFV}: CSF in the third and fourth ventricle, CSF_{CM}: CSF in the cisterna magna, CSF_{SAS_LUMBAR}: CSF in the subarachnoid space and lumbar region, Q_{CBF}: cerebral blood flow, Qt_{BBB}: transcellular diffusion clearance at the BBB, Qp_{BBB}: paracellular diffusion clearance at the BBB, Qt_{BCSFB1}: transcellular diffusion clearance at the BCSFB1, Qp_{BCSFB1}: paracellular diffusion clearance at the BCSFB1, Qt_{BCSFB2}: transcellular diffusion clearance at the BCSFB2, Qp_{BCSFB2}: paracellular diffusion clearance at the BCSFB2, Q_{BCM}: passive diffusion clearance at the brain cell membrane, Q_{LYSO}: passive diffusion clearance at the lysosomal membrane, Q_{ECF}: $brain_{ECF}$ flow, Q_{CSF}: CSF flow, AFin1-3: asymmetry factor into the CNS compartments 1-3, AFout1-3: asymmetry factor out of the CNS compartments 1-3, PHF1-7: pH-dependent factor 1-7, BF: binding factor.

Table I. Summary of human plasma, brain and CSF data sources for the PBPK model evaluation

		Acetaminophen			Oxycodone	Morphine		Phenytoin
		Study A1	Study A2	Study A3	Study O1	Study M1	Study M2	Study P1
Study design								
Condition of patients		Healthy subjects	Patients with nerve-root compression	Patients with traumatic brain injury	Patients undergoing elective gynecological surgery	Patients with traumatic brain injury	Patients with traumatic brain injury	epileptic patients
Nr of subjects		1 (mean values)	1 (mean values)	7	12	2	1	6
Dosage		1 g, 15 min infusion	2g (propacetamol), short infusion	1 g, 30 min infusion	0.1 mg/kg, 5min infusion	10 mg, 10min infusion	10 mg, 10min infusion	13 mg/kg, 100mg/min
Nr of samples (sampling time, h)	plasma	8 (0-6h)	11 (0-12h)	38 (0-6h)	133 (0-24h)	23 (0-3h)	11 (0-3h)	24 (0-1.25h)
	$brain_{ECF}$ [a] or CSF	8 (0-6h)	11 (0-13h)	54 (0-5.5h)	116 (0-24h)	74 (0-3h)	37 (0-3h)	20 (0-1.25h)
Data								
plasma		X	X	X	X	X	X	X
$brain_{ECF}$						X[e], X[f]	X[e], X[f]	
CSF_{EVD} [b]				X				
CSF_{SAS_LUMBAR} [c]		X	X		X			X
data references		(18)	(17)	(19)	(21)	(24)	(25)	(26)
fu,p [d]		85%			59%	-	-	13%
fu,p references		(20)			(22)(23)			(27)

[a] brain extracellular fluid compartment, [b] compartment of cerebrospinal fluid in EVD, [c] compartment of cerebrospinal fluid in subarachnoid space and lumbar region, [d] free fraction in plasma, [e] better side of brain tissue, [f] injured side of brain tissue

blue: data was obtained under physiological CNS conditions, red: data was obtained under pathophysiological CNS conditions

Scaling of the rat CNS PBPK model to humans

The previously developed rat CNS PBPK model (15) (**Figure 1**) consists of nine compartments, being plasma, brain microvessels ($brain_{MV}$), $brain_{ECF}$, $brain_{ICF}$, lysosomes, CSF_{LV}, CSF in the third and fourth ventricle (CSF_{TFV}), CSF in the cisterna magna (CSF_{CM}) and CSF_{SAS_LUMBAR}. The model parameters are either system- or drug-specific.

This rat CNS PBPK model was scaled to humans by 1) substitution of the rat system-specific parameters values by their corresponding human equivalents, 2) rat to human conversion of the contribution of active transport at the BBB and the BCSFB based on reported differences in the expression of active transporters, and 3) adding the rate of drug dispersion in the CNS.

System-specific parameters

Literature values were used for the physiological volumes for all CNS compartments, CBF, $brain_{ECF}$ bulk flow, CSF flow, surface area (SA) of the BBB (SA_{BBB}), SA of the BCSFB (SA_{BCSFB}), the ratio of SA_{BBB} and SA_{BCSFB} for transcellular and paracellular diffusion, the diameter of brain parenchyma cells, the diameter of lysosomes, the cross-width of the BBB cells and the effective pore size (29–44). The SA_{BCFSB} was divided into SA_{BCSFB1} which is the SA around CSF_{LV}, and SA_{BCSFB2} which is SA around CSF_{TFV}, like those in the rat CNS PBPK model (15). The total volume of lysosomes was calculated using the volume ratio of the lysosomes to the brain intracellular fluid of brain parenchyma cells (1:80) (45). The SA of total brain parenchymal cell membrane and the SA of total lysosomes were calculated using the diameter of brain parenchyma cells and the volume of $brain_{ICF}$, and diameter of lysosomes and the total volume of lysosomes, respectively. The values of the system-specific parameters used in the model are summarized in **Table II**.

Drug-specific parameters

The calculation of drug-specific parameters including the aqueous diffusivity coefficient and BBB transmembrane permeability of the compound was performed as described previously (15) and the details for the calculation are described in **Supplementary Material S1.** The influence of the net effect of active transporters on the drug exchange at the BBB and BCSFB was incorporated into the model using three asymmetry factors (AFin1-3 or AFout1-3, which can be calculated from Kp,uu values (unbound brain/CSF-to-plasma concentration ratio), such that they produced the same Kp,uu values within the model). If the net transport is influx of the drug, AFin1-3 were used, while AFout1-3 were fixed to 1. If the net transport is efflux of the drug, AFout1-3 were used, while AFin1-3 were fixed to 1 (15).

Table II. System-specific parameters of the human PBPK model in healthy condition

Description		Parameter	Human value	Reference
Volumes	Brain	V_{tot}	1400 mL	(29)
	$Brain_{ECF}$	$Vbrain_{ECF}$	240- 280mL (260 was used in the model)	(30,31)
	$Brain_{ICF}$	$Vbrain_{ICF}$	960 mL	(31)
	Total lysosome	V_{LYSO}	12 mL	calculated [d]
	CSF_{LV}	$VCSF_{LV}$	20-25 mL (22.5 was used in the model)	(32,33)
	CSF_{TFV}	$VCSF_{TFV}$	20-25 mL (22.5 was used in the model)	(32,33)
	CSF_{CM}	$VCSF_{CM}$	7.5 mL	(34,35)
	CSF_{SAS_LUMBAR}	$VCSF_{SAS\_LUMBAR}$	90-125 mL (90 was used in the model)	(32,33)
	Brain microvascular	V_{MV}	150 mL	(42)
Flows	Cerebral blood flow	Q_{CBF}	610-860 mL/min (735 was used in the model)	(36–38)
	$Brain_{ECF}$ bulk flow	Q_{ECF}	0.15-0.2 mL/min (0.175 was used in the model)	(39)
	CSF flow	Q_{CSF}	0.3–0.4 mL/min (0.35 was used in the model)	(39)
Surface areas	BBB	SA_{BBB}	12-18 m^2 [a] (12 was used in the model)	(40,41)
	BCSFB	SA_{BCSFB}	6-9 m^2 [b,c] (7.5 was used in the model)	calculated (assumed 50% of BBB_{SA})
	Total BCM	SA_{BCM}	228 m^2	calculated [e]
	Total lysosomal membrane	SA_{LYSO}	180 m^2	calculated [f]
Width	BBB	$Width_{BBB}$	0.3-0.5 µm (0.5 was used in the model)	(43)
effective pore size	BBB		0.0007-0.0009 µm (0.0007 was used in the model)	(44)

CSF, cerebrospinal fluid; BBB, blood-brain barrier; BCSFB, blood-cerebrospinal barrier; BCM, brain cell membrane
[a] 99.8 % of SA_{BBB} was used for transcellular diffusion, and 0.004 % of SA_{BBB} was used for paracellular diffusion, [b] 99.8 % of SA_{BCSFB} was used for transcellular diffusion and 0.016 % of SA_{BCSFB} was used for paracellular diffusion, [c] SA_{BCSFB1} and SA_{BCSFB2} was both assumed to be 3.75cm^2, [d] based on the volume ratio of lysosomes to $brain_{ICF}$ (1:80), [e] based on the number of brain parenchyma cells which was calculated using the total $brain_{ICF}$ volume and diameter of each brain parenchyma cell (15 µm) (46), [f] based on the lysosome number per cell which was calculated using the total lysosomal volume and diameter of each lysosome (0.5-1.0 µm) (47).

As no direct information is available on the values of AFs for human, we used two different approaches to obtain the values depending on the information available for the active transporters for each compound. We propose a workflow and decision tree to obtain human AF values for the individual compounds, based on availability of literature information (**Figure 2**), as follows:

1) A literature search was performed for the main transporters involved in the BBB/BCSFB transport of the compounds in humans.
2) If relevant active transporters were reported, a literature search was performed on species differences in transporter protein expression / activity of the main active transporters.
3) If information on the inter-species differences was available, rat AF values were converted to human AF values using a conversion factor as calculated from the differences in transporter protein expression and/or activity of the main active transporters between rats and humans (**Method 1**).

4) If information of the inter-species differences was not available for the compound, we searched information available from other compounds whose transfer are predominantly mediated by the same transporters, and then step 2 was repeated (**Method 2**).
5) If an active transporter was not reported, we searched for *in vitro* data able to derive the net contribution of active transport component on the overall permeability. If no indications of active transport could be found, the human AF values were fixed to 1 (**Method 3**). The details of the calculation methods to obtain human AF values from the *in vitro* data are described in **Supplementary Material S3.**

Below we describe in detail the rationale for selection of AF values for each compound.

- *Acetaminophen*

Acetaminophen is reported to be transported across the human BBB by passive diffusion only, (48), therefore we fixed the AF values for acetaminophen to 1 (**Method 3**).

- *Oxycodone*

An active influx transporter for oxycodone at the BBB has been reported; pyrilamine-sensitive proton-coupled organic cation (H+/OC) antiporter (49,50). Even though information on species difference in its protein expression level and its activity is not directly available for oxycodone, the transporter activity can be deduced from the *in vitro* observations on pyrilamine transfer, of which the exchange at the BBB is predominantly mediated by this transporter (49,50). Therefore, **Method 2** was applied for oxycodone. According to the *in vitro* studies on pyrilamine in the human BBB model (hCMEC/D3 cells), the Km and Vmax values of active uptake are comparable to those in the rat BBB model (TR-BBB13 cells) (50). Moreover, the weaker active uptake of oxycodone comparing to that of pyrilamine in the human BBB model (50) is in line with the observations in the rat BBB model (49). It thus appears reasonable to assume that the BBB influx mediated by this transporter is comparable between rat and human, and therefore the human AFs were considered to be similar to rat AFs. The human AF at the BBB, AFin1, was 2.3, which was calculated using a $Kpuu,brain_{ECF}$ (unbound $brain_{ECF}$-to-plasma concentration ratio) value of 1.7 (51). The human AFs at the BCSFB, AFout2 and AFout3, were assumed to be 1.9 and 2.3, respectively, which were calculated from a Kpuu,CSF (unbound CSF-to-plasma concentration ratio) value of 1 (21).

- *Morphine*

Permeability glycoprotein (P-gp) and multidrug resistance-associated proteins (MRPs) are reported to be the active efflux transporters for morphine at the rat BBB (52,53). Furthermore, an involvement of active influx transporters has also been suggested in rat

BBB (54). Even though morphine is reported to be a substrate of P-gp (55) for humans, other efflux and influx transporters have not been clearly identified. The P-gp protein concentration in rat brain endothelial cells is about 19 fmol/mg protein, which is about three-fold higher than that in humans (6 fmol/mg protein) (56). Regarding the P-gp activity for morphine, no inter-species difference has been observed (57). Therefore, the rat-to-human conversion factor of AFs was set to 3 for morphine. The rat AFout1, AFout2 and AFout3 are 20, 38 and 49, respectively (15), and therefore in this study human AFout1, AFout2 and AFout3 were assumed to be 6.6, 13 and 16, respectively (**Method 1**).

- *Phenytoin*

P-gp and MRPs are suggested to be the active efflux transporters for phenytoin at the rat BBB (58,59). However, many *in vitro* studies, including the studies using human hCMEC/D3 cells and other cells expressing human P-gp and human MRPs, have shown that phenytoin is neither a substrate for human P-gp nor human MRP2 (60–63). Even though the reasons for these differences between the *in vivo* rat studies and the *in vitro* experiments using human P-gp and MRPs are not clear, inter-species differences in the activity by P-gp for phenytoin (63) and MRP2 have been reported (64). Therefore, **Method 3** was applied to predict AFs for phenytoin. In this study, we assumed that the human AFs for phenytoin are equal to 1.

Use of system-specific and drug-specific parameters in the model

Drug transport at the BBB and BCSFB, brain cellular distribution, acidic subcellular distribution and drug binding were derived by using drug-specific parameter values and system-specific parameters using the equations which were described previously (15) and are provided in **Supplementary Material S2**.

Scaling of the dispersion rate

Previously the values of the system-specific drug dispersion rate within the brain and CSF have been estimated based on rat microdialysis data of nine compounds (19). This dispersion rate is defined as a combination of CSF flow, $brain_{ECF}$ bulk flow and turbulence flow of the drug molecules. For the scaling of the drug dispersion rate to humans we used the following allometric scaling equation.

$$P_{human} = P_{rat} \times \left(\frac{BW_{human}}{BW_{rat}}\right)^{0.75} \quad (1)$$

where P_{human} is the scaled human parameter, P_{rat} is the estimated rat parameter from the model, BW_{human} is the average human body weight (75 kg), and BW_{rat} is the average rat body weight (250 g).

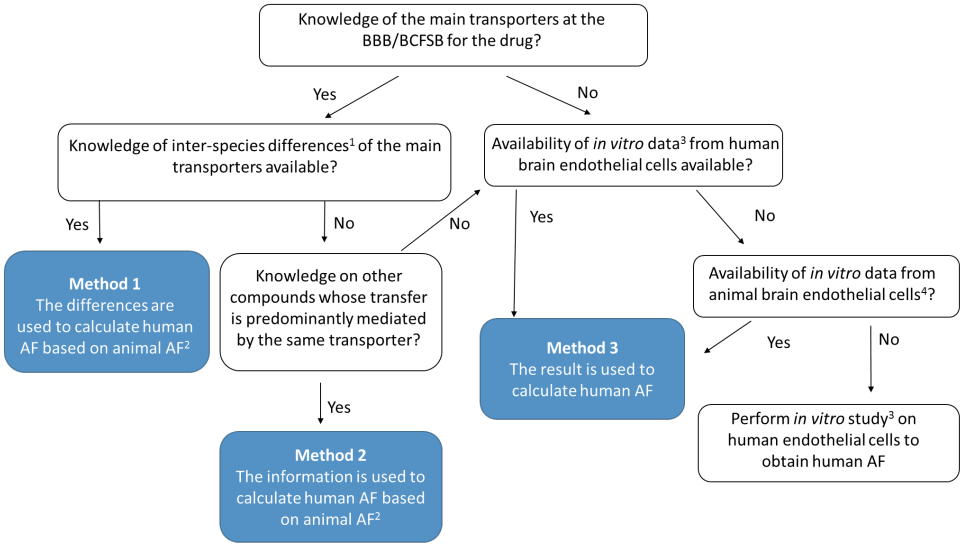

1. Inter-species differences of the expression level and activity/function of the main transporters, are needed.
2. The methods to calculate the rat AF were reported (15). In short, rat AF was calculated using the Kp,uu values which were obtained from *in vivo* studies or *in silico* predictions.
3. *In vitro* data which is able to derive active transport component of the overall permeability are needed. The details are provided in supplementary material S3.
4. The assumption is made that the overall active transport characteristics of animal and human BBB are similar.

Figure 2. Decision tree to obtain human AF.

Evaluation of the human CNS PBPK model

The predictions of the scaled human CNS PBPK model were evaluated by comparing of model predictions to observed human PK data in $brain_{ECF}$, CSF_{SAS_LUMBAR} and/or CSF_{EVD}. The accuracy of the prediction was evaluated with symmetric mean absolute percentage error (SMAPE) (Eq. 2) using population prediction (PRED). We also performed 200 simulations for each compound, then calculated 2.5 % tile, median and 97.5 % tile of the simulated concentrations and plotted these together with the observations.

$$SMAPE = \frac{1}{N}\sum_{k=1}^{N}\left|\frac{Y_{OBS,ij}-Y_{PRED,ij}}{(Y_{OBS,ij}+Y_{PRED,ij})/2}\right| \times 100 \quad (2)$$

where $Y_{OBS,ij}$ is the *j*th observation of the *i*th subject, $Y_{PRED,ij}$ is the *j*th mean prediction of the *i*th subject, and N is the number of observations.

Simulated impact of different pathophysiological conditions on CNS PK

Under pathophysiological CNS conditions, several CNS system-specific parameter values, such as CBF, BBB characteristics, BCSFB characteristics, $brain_{ECF}$ bulk flow, CSF flow and active transporters, have been reported to be changed (**Supplemental Table SI**). The following data were available from literature: acetaminophen concentrations in CSF_{EVD} and morphine concentrations in $brain_{ECF}$ which were obtained from TBI patients, and phenytoin data in CSF_{SAS_LUMBAR} which were obtained from epileptic patients (**Table I**).

In TBI patients, a decrease in CBF, an increase in paracellular permeability due to the disruption of the tight junction complexes, and changes in activity/expression of active transporters (such as a decreased expression of P-gp) have been reported (65–67). For epileptic conditions, studies have indicated regional decreases in CBF, increased paracellular permeability due to the opening of the tight junction proteins, and an increase in some active efflux transporters such as P-gp and MRPs (68–71).

To investigate the impact of such pathological changes on each compound's PK profiles, we simulated the PK upon such changes. In the simulations, the system-specific parameter values were varied within a range of 20-500% of their original values (i.e. 5 times lower or higher).

If the changes in the values of the system-specific parameters had a relevant impact on PK profiles, the model predictions were performed again by adapting values of system-specific parameters identified in the literature, and subsequently compared to the observed PK data.

RESULTS

Plasma PK parameter values

The plasma PK parameters used in the analysis for acetaminophen, morphine, oxycodone, and phenytoin are summarized in **Supplemental Table SII.** For acetaminophen (study A3) and morphine (study M1 and M2), the plasma PK parameter values were obtained from literature (19). For acetaminophen (study A1 and study A2), oxycodone (study O1) and phenytoin (study O1), the descriptive plasma PK model was developed using available plasma data. The plasma PK parameter values were obtained with acceptable precision (relative standard error <66%) and could adequately describe the plasma PK data (**Figure 3** and **Figure 5**).

Prediction of CNS PK in physiological CNS conditions

System-specific and drug-specific parameters in physiological CNS conditions are summarized in **Table II** and **Table III**, respectively**.** The parameters derived from human system-specific and drug-specific parameters are summarized in **Table IV**. The drug dispersion rate for human was calculated to be 1.6 mL/min based on allometric scaling. The model could adequately predict the PK profiles in $brain_{ECF}$ for morphine and the PK profiles in CSF_{SAS_LUMBAR} for acetaminophen and oxycodone under physiological CNS conditions (**Figure 3**), with an SMAPE of $brain_{ECF}$ and CSF_{SAS_LUMBAR} of 49% and 54%, respectively.

Prediction of CNS PK in TBI and epileptic conditions

To explore the impact of each system-specific parameters, which were altered in pathological CNS conditions of TBI and epilepsy on the PK profiles for acetaminophen, morphine and phenytoin, simulations were performed by changing the values of the CBF, and paracellular diffusion. The influence of the active efflux transporters was also simulated for morphine. The impact on model predictions after changing the values of CBF, paracellular diffusion and the influence of the active efflux transporters within a range of 20-500% of their original values are shown in **Figure 4**. It can be seen that the impact of pathological changes on PK profiles is drug-dependent and CNS compartment-dependent. For acetaminophen, the PK profiles in CSF_{LV} were not sensitive to the changes in CBF nor to the changes in paracellular diffusion across the BBB/BCSFB. In contrast, for morphine $brain_{ECF}$ concentrations increased with an increase in paracellular diffusion, and decreased with an increase in active efflux transport. For phenytoin, no change was observed in PK profiles in CSF_{SAS_LUMBAR} with the changes in CBF and paracellular diffusion.

Since TBI and epilepsy conditions did not influence acetaminophen PK profiles in CSF_{LV} and phenytoin PK profiles in CSF_{SAS_LUMBAR} to a significant extent, the model prediction for these PK data was performed using the physiological values of the system-specific parameters (**Figure 5**). The model predictions captured the acetaminophen PK data in CSF_{EVD} and the phenytoin PK data in CSF_{SAS_LUMBAR} well even if the concentrations are slightly over-predicted around the early sampling time for the acetaminophen PK data in CSF_{EVD}.

On the other hand, we found that the values of paracellular diffusion and the influence of the active efflux transporters needed to be adjusted to capture the morphine concentrations in $brain_{ECF}$ in TBI patients (**Figure 4**). Morphine PK data in $brain_{ECF}$ in TBI patients were captured well when paracellular diffusion was upregulated and active efflux transport was downregulated (**Figure 6**).

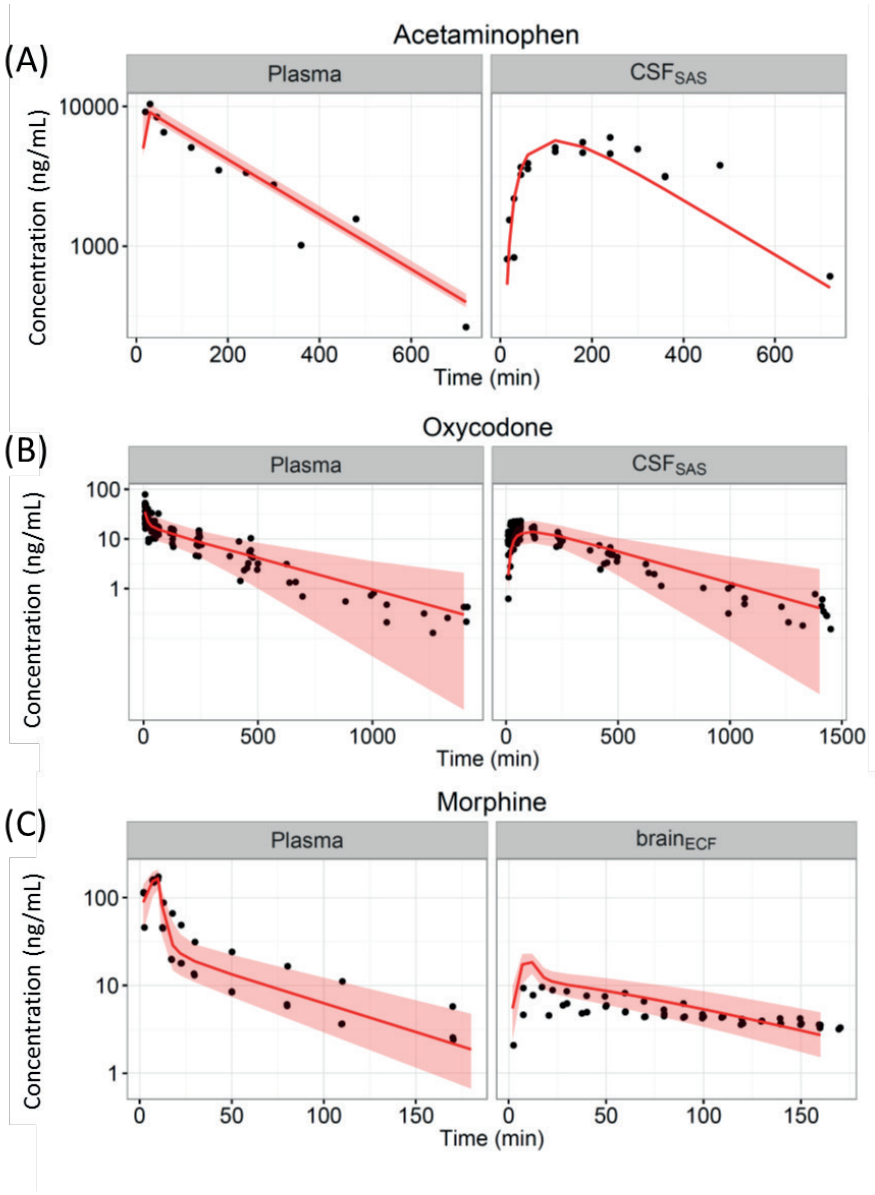

Figure 3. Predicted (red lines: median, shaded area is 95 % prediction interval) and observed (circles) concentration-time profiles in physiological CNS compartments. (A) Plasma and CSF in the lumbar region (CSF_{SAS_LUMBAR}) data for acetaminophen which were obtained from both healthy subjects and patients with nerve-root compression, (B) plasma and CSF_{SAS_LUMBAR} data for oxycodone which were obtained from patients undergoing elective gynecological surgery and (C) plasma and $brain_{ECF}$ data for morphine which were obtained from the uninjured side of the brain in traumatic brain injury (TBI) patients. The x-axis represents the time in minutes and the y-axis represents the concentration in ng/mL.

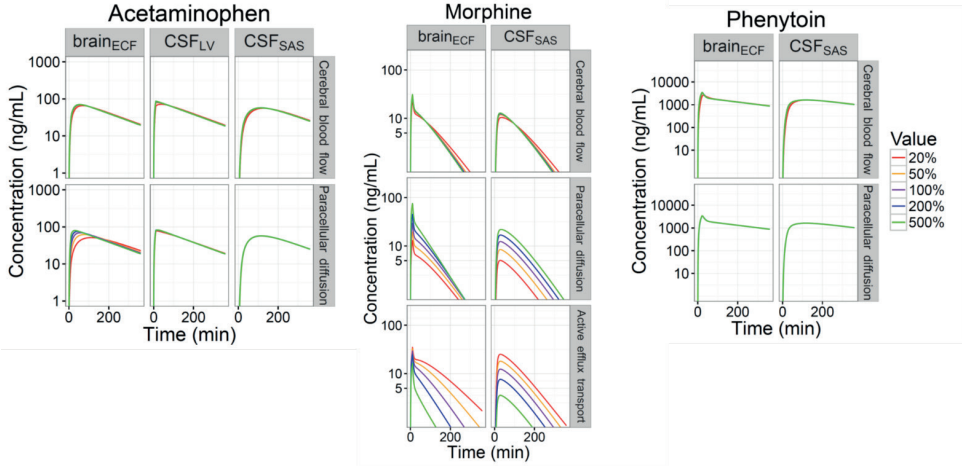

Figure 4. Simulation of the concentration-time profiles for acetaminophen, morphine and phenytoin using the human CNS PBPK model. The values of CBF, paracellular diffusion and an influence of active transports (if applicable) were varied within the range of 20-500% of their original values (colors). The plots were stratified by the CNS compartments (panels). The x-axis represents the time in minutes and the y-axis represents the concentration in ng/mL.

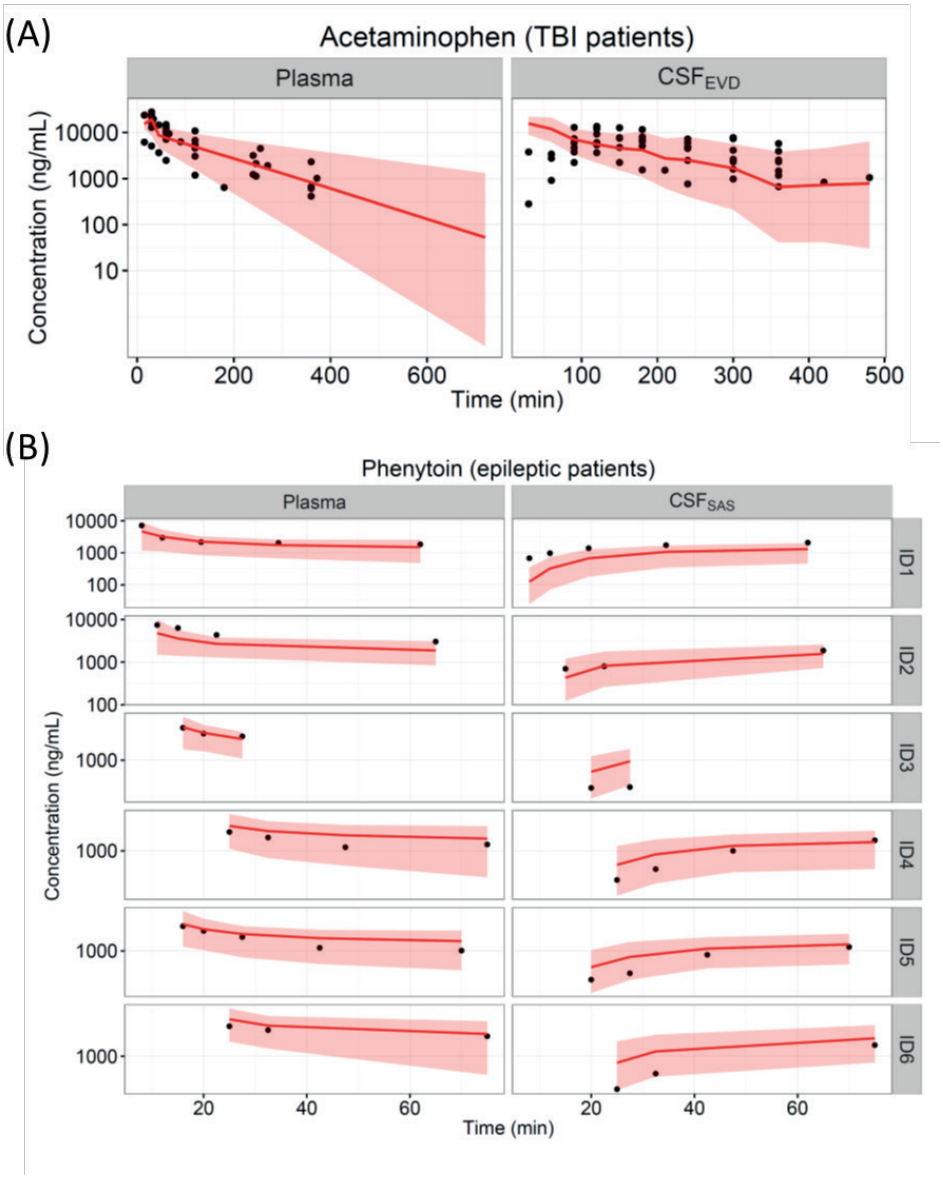

Figure 5. Model prediction (red lines: median, shaded area is 95% prediction interval) versus concentration-time profiles (circles) for each pathophysiological condition. (A) Acetaminophen data was obtained from plasma and CSF in the lateral ventricle collected by extra-ventricular drainage (CSF_{EVD}) from traumatic brain injury (TBI) patients, (B) phenytoin data was obtained from plasma and CSF in the lumbar region (CSF_{SAS_LUMBAR}) from epileptic patients. The x-axis represents the time in minutes and the y-axis represents the concentration in ng/mL.

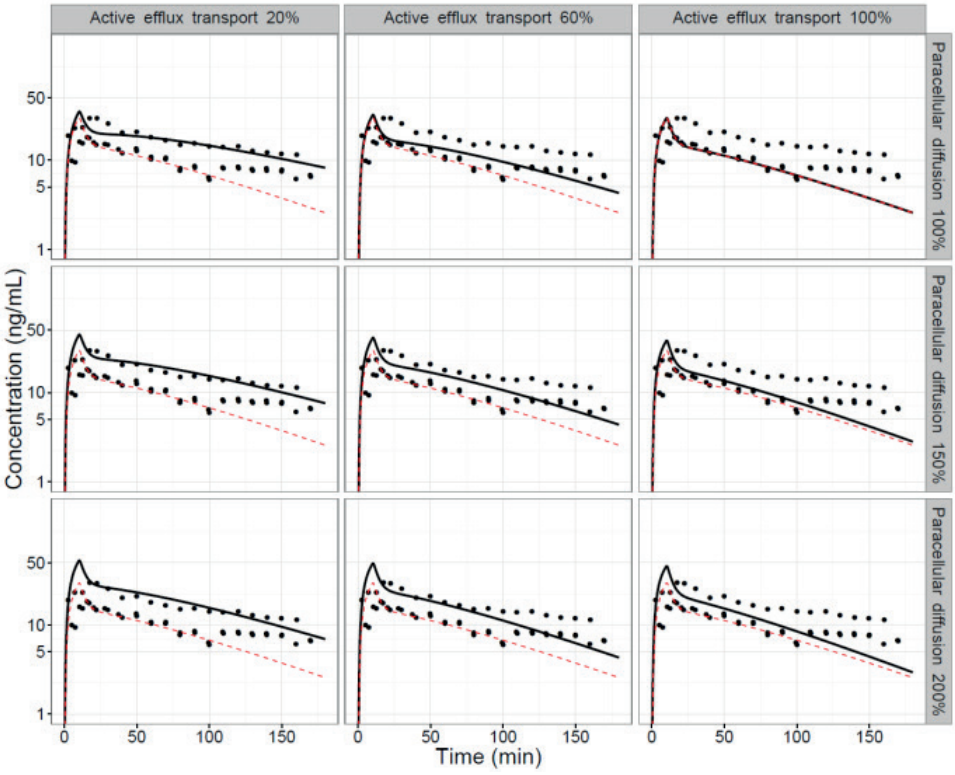

Figure 6. Model prediction (black lines) versus concentration-time profiles (circles) for morphine in brain$_{ECF}$ in TBI patients. The plots were stratified by the change in the values of the system-specific parameters. The red dotted lines were the model predicted concentration-time profile for morphine in brain$_{ECF}$ in healthy subjects. The x-axis represents the time in minutes and the y-axis represents the concentration in ng/mL.

Table III. Drug-specific parameters of the PBPK model

			Acetaminophen	Oxycodone	Morphine	Phenytoin
Drug specific parameters						
Transmembrane permeability		cm/min	$1.1*10^{-4}$	$3.5*10^{-4}$	$2.5*10^{-4}$	0.0077
Aqueous diffusivity coefficient (Paracellular diffusion)		cm^2/min	$4.6*10^{-4}$	$3.3*10^{-4}$	$3.4*10^{-4}$	$3.6*10^{-4}$
AF	AFin1		1	2.3	1	1
	AFin2		1	1	1	1
	AFin3		1	1	1	1
	AFout1		1	1	6.6	1
	AFout2		1	1.9	13	1
	AFout3		1	2.3	16	1
Free fraction						
fu,p			0.85	0.59	0.11	0.13
fu,b			-	0.39 (72)	0.45 (72)	-
Physicochemical properties						
Molecular weight			151	315	285	252
log P			0.5	0.3	0.9	2.5
pKa (Acid)			9.5	13.6	10.3	9.5
pKa (Base)			-4.4	8.2	9.1	-9.0
Charge class			Neutral	Base	Base	Neutral

AF, asymmetry factor
AFin1-3 and AFout1-3 were converted from the rat AFs or obtained from *in vitro* study.

Table IV. Parameters derived using system-specific and drug-specific parameters in the PBPK model

Parameter	Unit	Acetaminophen	Oxycodone	Morphine	Phenytoin
Q_{BBB_in}	mL/min	72	120	64	510
Q_{BBB_out}	mL/min	72	68	130	510
Qt_{BBB}	mL/min	6.5	21	15	460
Qp_{BBB}	mL/min	66	47	50	52
PHF1		1.0	0.82	0.80	1.0
Q_{BCSFB1_in}	mL/min	57	47	46	190
Q_{BCSFB1_out}	mL/min	57	46	98	190
Qt_{BCSFB1}	mL/min	2.0	6.6	4.7	140
Qp_{BCSFB1}	mL/min	55	39	41	43
PHF2		1.0	0.82	0.80	1.0
Q_{BCSFB2_in}	mL/min	57	47	46	190
Q_{BCSFB2_out}	mL/min	57	46	98	190
Qt_{BCSFB2}	mL/min	2.0	6.6	4.7	140
Qp_{BCSFB2}	mL/min	55	39	41	43
PHF3		1.0	0.82	0.80	1.0
Q_{BCM_in}	mL/min	250	650	461	18000
Q_{BCM_out}	mL/min	250	360	230	18000
PHF4		1.0	0.82	0.80	1.0
PHF5		1.0	0.43	0.40	1.0
Q_{LYSO_in}	mL/min	120	170	120	8800
Q_{LYSO_out}	mL/min	130	1.8	1.2	8900
PHF6		1.0	0.43	0.40	1.0
PHF7		1.0	0.0046	0.0041	1.0
BF		-	0.01	1	-

$Q_{BBB\_in} = Qp_{BBB} + Qt_{BBB}$*AFin1, $Q_{BBB\_out} = (Qp_{BBB} + Qt_{BBB}$*AFout1)*PHF1,
Qp_{BBB}= (Aqueous diffusivity coefficient/$Width_{BBB}$)*SA_{BBBp},
Qt_{BBB}= 1/2*Transmembrane permeability*SA_{BBBt}
$Q_{BCSFB1\_in} = Qp_{BCSFB1} + Qt_{BCSFB1}$*AFin2,
$Q_{BCSFB1\_out} = (Qp_{BCSFB1} + Qt_{BCSFB1}$*AFout2)*PHF2,
Qp_{BCSFB1}= (Aqueous diffusivity coefficient/$Width_{BCSFB1}$)*$SA_{BCSFB1p}$,
Qt_{BCSFB1}= 1/2* Transmembrane permeability *$SA_{BCSFB1t}$
$Q_{BCSFB2\_in} = Qp_{BCSFB2} + Qt_{BCSFB2}$*AFin3,
$Q_{BCSFB2\_out} = (Qp_{BCSFB2} + Qt_{BCSFB2}$*AFout3)*PHF3,
Qp_{BCSFB2}= (Aqueous diffusivity coefficient/$Width_{BCSFB2}$)*$SA_{BCSFB2p,}$
Qt_{BCSFB2}= 1/2* Transmembrane permeability *$SA_{BCSFB2t}$
Q_{BCM_in}= Transmembrane permeability *SA_{BCM}*PHF4,
Q_{BCM_out}= Transmembrane permeability *SA_{BCM}*PHF5
Q_{LYSO_in}= Transmembrane permeability *SA_{LYSO}*PHF6,
Q_{LYSO_in}= Transmembrane permeability *SA_{LYSO}*PHF7
PHF1, PHF2, PHF3, PHF4, PHF5, PHF6, and PHF7 were calculated from the pKa of each compound and pH of the respective compartment.
BF was calculated from the Kp of each compound.

DISCUSSION

We developed a human CNS PBPK model to predict unbound drug PK of four model compounds in multiple CNS compartments. Under physiological CNS conditions, good predictions of observed human data were achieved within a 1.6-fold error. Furthermore, the model showed its ability to be used for building a better understanding of the key system properties that may explain the changes on drug concentration-time profiles under pathophysiological CNS conditions.

The human CNS PBPK model can be applied to any (existing or new) compounds once the physicochemical properties and information on the involvement of active transporters at the BBB and the BCSFB are available. Such information can be obtained from *in silico* predictions and/or *in vitro* studies.

The model uses plasma PK data as input to build a plasma PK model. In our study we either used plasma PK models that have been published or we developed the plasma PK model separately on the basis of existing plasma PK data. It should be noted that even in the absence of a plasma PK model or data, the CNS PBPK model can be used in conjunction with plasma PK simulations by using the existing whole-body PBPK platforms. Thus, the human CNS PBPK model does not require any *in vivo* data to predict unbound drug PK at target-site in the human CNS.

Gathering as much information as possible about unbound drug PK in the CNS is important to improve CNS drug development and CNS drug treatment, because it is the driver for drug-target binding kinetics and therewith for the drug effect profile. In contrast to the *ex vivo* techniques, such as brain homogenate and brain slicing techniques, as well as *in silico* approaches like quantitative structure-activity relationship models (73,74) that can provide information on unbound concentrations in the brain at steady state conditions, the CNS PBPK model predicts the unbound drug concentration time course. This is an important improvement since even during chronic dosing, variations in drug concentrations will still be present and may influence the target occupancy-time profile (75).

The human CNS PBPK model allows prediction of the unbound drug PK in multiple physiologically relevant CNS compartments. This is crucial as the PK profiles in different CNS compartments are known to be different, even for drugs that are not subjected to active transport (9). Moreover, the model could be used to investigate the impact on PK profiles in the different CNS compartments as a result of pathological processes, which have shown to be drug-dependent as well as CNS compartment-dependent (**Figure**

5 and 6). To our best knowledge, such integration of multiple aspects has not been reported earlier, and it will substantially contribute to an increased insight into CNS PK changes in pathological conditions in relation to the CNS effects.

A key feature of drug transport across the BBB and BCSFB is the contribution of active transporters. In PBPK modeling, expression levels and activity of each active transporter should ideally be separately incorporated. The major transporters such as P-gp and MRP are investigated well with regard to their inter-species differences of expression levels and transporters activity; however, such information is currently lacking for the other transporters (56,76).

Therefore, in our human CNS PBPK model, instead of using information on individual transporters, we used the "net contribution of the active transport" approach. This is a useful approach in situations where active transporters, which have not yet been widely investigated, are involved in the process of drug exchange at the BBB/BCSFB. In this study, we investigated a method to convert the "net contribution of the active transport (AFs)" at the BBB and BCSFB from rat to human, or obtain it from *in vitro* studies. We propose a workflow and decision tree to derive human "net contribution of the active transport (AFs)" (**Figure 2**).

In the rat PBPK model, we derived the "net contribution of the active transport (AFs)" from Kpuu values (15). The translation method of AFs values from rat to human depends on the available information about the transporters involved in the processes. If the existing literature information is not sufficient to support the conversion of the rat AFs to human AFs, we proposed alternative methods to obtain human AFs directly from *in vitro* study using preferably human brain endothelial cells, such as hCMEC/D3 cells. Thus, either way, theoretically we do not need any *in vivo* data to obtain human AFs.

We have shown the potential of the model to be adapted according to literature information of pathophysiological changes and to explore the impact of the pathophysiological changes on PK profiles in each CNS compartment. For PK data for acetaminophen in CSF_{EVD} under TBI condition and PK data for phenytoin in CSF_{SAS_LUMBAR} under epileptic conditions, the impact of the conditions did not lead to significant alterations of CNS PK, hence no changes to the model were needed to obtain reasonable predictions. For morphine, the simulations showed that the model could describe the drug concentration in $brain_{ECF}$ in TBI patients if the paracellular diffusion at the BBB and BCSFB was increased by more than 50% and AFs at the BBB and BCSFB were decreased by more than 40%. Our findings align with the reported 40% decrease in expression of P-gp in TBI patients (67). This demonstrates how the model could provide quantitative

mechanistic insights of clinically observed alterations in CNS PK which are supported by additional external evidence. In the future, additional human data, for example from the accessible CSF lumbar region, can provide further information to validate the model in other pathophysiological conditions, and can better inform the human CNS PBPK model about what system-specific parameter values has actually changed or how much the system-specific parameter values need to be adjusted.

Due to the lack of information for the drug dispersion rate in the CSF, we used allometric scaling of the drug dispersion rate in rats using body weight to obtain the drug dispersion rate for humans. Since the drug dispersion rate may be different depending on the physiological components such as the length of spine and size of the tube of spine, an allometric scaling can be considered as an appropriate approach to scale the value among species. In this study, the average drug dispersion rate value in rat for the nine compounds was used for the scaling (19). At least for acetaminophen, oxycodone, morphine and phenytoin, the average drug dispersion rate was sufficient to capture the PK profiles of the compounds in the CNS. However, the drug dispersion rate may depend on not only the physiological components (which have already been taken into account by the allometric scaling), but also on the physicochemical properties such as molecular weight and lipophilicity. Therefore, further investigations are needed to optimize the drug dispersion rate for each compound in human.

CONCLUSIONS

A human CNS PBPK model was developed to predict the concentration-time profiles of four model compounds in human CNS compartments. All model parameters were either derived from *in silico* predictions, literature data or based on *in vitro* information. Therefore, the model can provide the concentration-time profiles in multiple physiologically relevant compartments in human CNS without the need of *in vivo* PK data. We demonstrated that the model could predict the $brain_{ECF}$ and CSF_{SAS_LUMBAR} concentrations-time profiles under physiological CNS conditions. We also showed how the model can provide quantitative understanding of the impact of pathophysiological conditions on PK profiles in each CNS location. This human CNS PBPK model provides the basis to link CNS PK with drug-target binding kinetics and the biological effect(s) of the drug. As such, the developed model will have a substantial role in the selection of CNS drug candidates, in the prediction of target-site concentrations in humans, and to support the assessment of drug efficacy and safety in the early stage of the drug development.

REFERENCES

1. Arrowsmith J, Miller P. Trial Watch: Phase II and Phase III attrition rates 2011–2012. Nat Rev Drug Discov. 2013;12(8):569–569.
2. Danhof M, de Jongh J, de Lange ECM, Della Pasqua O, Ploeger BA, Voskuyl RA. Mechanism-Based Pharmacokinetic-Pharmacodynamic Modeling: Biophase Distribution, Receptor Theory, and Dynamical Systems Analysis. Annu Rev Pharmacol Toxicol. 2007;47(1):357–400.
3. Westerhout J, Danhof M, de Lange ECM. Preclinical Prediction of Human Brain Target Site Concentrations : Considerations in Extrapolating to the Clinical Setting. J Pharm Sci. 2011;100(9):3577–93.
4. Deo AK, Theil F-P, Nicolas J-M. Confounding parameters in preclinical assessment of blood-brain barrier permeation: an overview with emphasis on species differences and effect of disease states. Mol Pharm. 2013;10(5):1581–95.
5. Yamamoto Y, Danhof M, de Lange ECM. Microdialysis : the Key to Physiologically Based Model Prediction of Human CNS Target Site Concentrations. AAPS J. 2017;19(4):891–909.
6. Kalvass JC, Maurer TS. Influence of nonspecific brain and plasma binding on CNS exposure: Implications for rational drug discovery. Biopharm Drug Dispos. 2002;23(8):327–38.
7. Friden M, Gupta A, Antonsson M, Bredberg U, Hammarlund-Udenaes M. In Vitro Methods for Estimating Unbound Drug Concentrations in the Brain Interstitial and Intracellular Fluids. Drug Metab Dispos. 2007;35:1711–9.
8. de Lange ECM, Danhof M, de Boer AG, Breimer DD. Critical factors of intracerebral microdialysis as a technique to determine the pharmacokinetics of drugs in rat brain. Brain Res. 1994;666(1):1–8.
9. Westerhout J, Ploeger B, Smeets J, Danhof M, de Lange ECM. Physiologically based pharmacokinetic modeling to investigate regional brain distribution kinetics in rats. AAPS J. 2012;14(3):543–53.
10. Westerhout J, Smeets J, Danhof M, de Lange ECM. The impact of P-gp functionality on non-steady state relationships between CSF and brain extracellular fluid. J Pharmacokinet Pharmacodyn. 2013;40(3):327–42.
11. Westerhout J, van den Berg D-J, Hartman R, Danhof M, de Lange ECM. Prediction of methotrexate CNS distribution in different species - Influence of disease conditions. Eur J Pharm Sci. 2014;57:11–24.
12. Dresel S, Tatsch K, Dahme I, Mager T, Scherer J, Hahn K. Iodine-123-Iodobenzamide SPECT assessment of dopamine D2 receptor occupancy in risperidone treated schizophrenia patients. J Nucl Med. 1998;39(7):1138–42.
13. Mamo D, Kapur S, Shammi CM, Papatheodorou G, Mann S, Therrien F, et al. A PET Study of Dopamine D2 and Serotonin 5-HT2 Receptor Occupancy in Patients with Schizophrenia Treated with Therapeutic Doses of Ziprasidone. Am J Psychiatry. 2004;161(5):818–25.

14. Neuwelt E, Abbott NJ, Abrey L, Banks WA, Blakley B, Davis T, et al. Strategies to advance translational research into brain barriers. Lancet Neurol. 2008;7(1):84–96.
15. Yamamoto Y, Välitalo PA, Huntjens DR, Proost JH, Vermeulen A, Krauwinkel W, et al. Predicting drug concentration-time profiles in multiple relevant CNS compartments using a comprehensive physiologically based pharmacokinetic model. in press. CPT Pharmacometrics Syst Pharmacol. 2017. In press
16. Beal S, Sheiner L, Boeckmann A, Bauer R. NONMEM User's Guides. Icon Development Solutions, Ellicott City. 2010.
17. Bannwarth B, Netter P, Lapicque F, Gillet P, Péré P, Boccard E, et al. Plasma and cerebrospinal fluid concentrations of paracetamol after a single intravenous dose of propacetamol. Br J Clin Pharmacol. 1992;34(1):79–81.
18. Singla NK, Parulan C, Samson R, Hutchinson J, Bushnell R, Beja EG, et al. Plasma and Cerebrospinal Fluid Pharmacokinetic Parameters After Single-Dose Administration of Intravenous, Oral, or Rectal Acetaminophen. Pain Pract. 2012;12(7):523–32.
19. Yamamoto Y, Välitalo PA, van den Berg D-J, Hartman R, van den Brink W, Wong YC, et al. A Generic Multi-Compartmental CNS Distribution Model Structure for 9 Drugs Allows Prediction of Human Brain Target Site Concentrations. Pharm Res. 2017;34(2):333–51.
20. Gazzard B, Ford-Hutchinson A, Smith M, Williams R. The binding of paracetamol to plasma proteins of man and pig. J Pharm Pharmacol. 1973;25(12):964–7.
21. Kokki M, Välitalo P, Kuusisto M, Ranta VP, Raatikainen K, Hautajärvi H, et al. Central nervous system penetration of oxycodone after intravenous and epidural administration. Br J Anaesth. 2014;112(1):133–40.
22. Dean M. Opioids in renal failure and dialysis patients. J Pain Symptom Manage. 2004;28(5):497–504.
23. Kirvela M, Lindgren L, Seppala T, Olkkola KT. The pharmacokinetics of oxycodone in uremic patients undergoing renal transplantation. J Clin Anesth. 1996;8(1):13–8.
24. Ederoth P, Tunblad K, Bouw R, Lundberg CJ, Ungerstedt U, Nordstrom CH, et al. Blood-brain barrier transport of morphine in patients with severe brain trauma. Br J Clin Pharmacol. 2003;57(4):427–35.
25. Bouw R, Ederoth P, Lundberg J, Ungerstedt U, Nordström C-H, Hammarlund-Udenaes M. Increased blood-brain barrier permeability of morphine in a patient with severe brain lesions as determined by microdialysis Case report. Acta Anaesthesiol Scand. 2001;45(3):390–2.
26. Wilder BJ, Ramsay RE, Willmore LJ, Feussner GF, Perchalski RJ, Shumate JB. Efficacy of intravenous phenytoin in the treatment of status epilepticus: Kinetics of central nervous system penetration. Ann Neurol. 1977;1(6):511–8.
27. Fraser DG, Ludden TM, Evens RP, Sutherland EW. Displacement of phenytoin from plasma binding sites by salicylate. Clin Pharmacol Ther. 1980;27(2):165–9.

28. Nguyen T-H-T, Mouksassi M-S, Holford N, Al-Huniti N, Freedman I, Hooker AC, et al. Model evaluation of continuous data pharmacometric models: Metrics and graphics. CPT pharmacometrics Syst Pharmacol. 2016;(1):1–20.

29. Dekaban A, Sadowsky D. Changes in brain weights during the span of human life: relation of brain weights to body heights and body weights. Ann Neurol. 1978;4(4):345–56.

30. Begley DJ, Bradbury MW, Kreuter J. The Blood-Brain Barrier and Drug Delivery to the CNS. New York: Marcel Dekker, Inc. 2000.

31. Thorne RG, Hrabe S, Nicholson C, Robert G. Diffusion of Epidermal Growth Factor in Rat Brain Extracellular Space Measured by Integrative Optical Imaging. J Neurophysiol. 2004;92(6):3471–81.

32. Sakka L, Coll G, Chazal J. Anatomy and physiology of cerebrospinal fluid. Eur Ann Otorhinolaryngol Head Neck Dis. 2011 Dec;128(6):309–16.

33. Pardridge WM. Drug transport in brain via the cerebrospinal fluid. Fluids Barriers CNS. 2011;8(7):1–7.

34. Robertson EG. Developmental defects of the cisterna magna and dura mater. J Neurol Neurosurg Psychiatry. 1949;12(1):39–51.

35. Adam R, Greenberg JO. The mega cisterna magna. J Neurosurg. 1978;48(2):190–2.

36. Stange K, Greitz M, Ingvar T, Hindmarsh T, Sollevi A. Global cerebral blood flow during infusion of adenosine in humans: assessment by magnetic resonance imaging and positron emission tomography. Acta Physiol Scand. 1997;160(2):117–22.

37. Ito H, Inoue K, Goto R, Kinomura S, Taki Y, Okada K, et al. Database of normal human cerebral blood flow measured by SPECT: I. Comparison between I-123-IMP, Tc-99m-HMPAO, and Tc-99m-ECD as referred with O-15 labeled water PET and voxel-based morphometry. Ann Nucl Med. 2006;20(2):131–8.

38. Fagerholm U. The highly permeable blood-brain barrier: an evaluation of current opinions about brain uptake capacity. Drug Discov Today. 2007;12(23–24):1076–82.

39. Kimelberg HK. Water homeostasis in the brain: basic concepts. Neuroscience. 2004 Jan;129(4):851–60.

40. Wong AD, Ye M, Levy AF, Rothstein JD, Bergles DE, Searson PC. The blood-brain barrier: an engineering perspective. Front Neuroeng. 2013;6:1–22.

41. Abbott NJ, Patabendige AAK, Dolman DEM, Yusof SR, Begley DJ. Structure and function of the blood-brain barrier. Neurobiol Dis. 2010;37(1):13–25.

42. Rengachary SS, Ellenbogen RG. Principles of Neurosurgery. Edinburgh: Elsevier Mosby; 2005.

43. Cornford EM, Hyman S. Localization of brain endothelial luminal and abluminal transporters with immunogold electron microscopy. NeuroRx. 2005;2(1):27–43.

44. Monteiro J, Goraksha S. 'ROSE concept' of fluid management: Relevance in neuroanaesthesia and neurocritical care. J Neuroanaesth Crit Care. 2017;4(1):10.

45. Loryan I, Sinha V, Mackie C, van Peer A, Drinkenburg W, Vermeulen A, et al. Mechanistic Understanding of Brain Drug Disposition to Optimize the Selection of Potential Neurotherapeutics in Drug Discovery. Pharm Res. 2014;32(8):2203–19.

46. Trapa PE, Belova E, Liras JL, Scott DO, Steyn SJ. Insights from an Integrated Physiologically Based Pharmacokinetic Model for Brain Penetration. J Pharm Sci. 2016;105(2):965–71.

47. Hardin J, Bertoni GP, Kleinsmith LJ. Becker's World of the Cell, 8th Edition. San Francisco: Pearson Education Inc.; 2011.

48. Mabondzo A, Bottlaender M, Guyot AC, Tsaouin K, Deverre JR, Balimane P V. Validation of in vitro cell-based human blood-brain barrier model using clinical positron emission tomography radioligands to predict in vivo human brain penetration. Mol Pharm. 2010;7(5):1805–15.

49. Okura T, Hattori A, Takano Y, Sato T, Hammarlund-udenaes M, Terasaki T, et al. Involvement of the Pyrilamine Transporter, a Putative Organic Cation Transporter, in Blood-Brain Barrier Transport of Oxycodone. Drug Metab Dispos. 2008;36(10):2005–13.

50. Shimomura K, Okura T, Kato S, Couraud P-O, Schermann J-M, Terasaki T, et al. Functional expression of a proton-coupled organic cation (H+/OC) antiporter in human brain capillary endothelial cell line hCMEC/D3, a human blood-brain barrier model. Fluids Barriers CNS. 2013;10(1):8.

51. Kitamura A, Okura T, Higuchi K, Deguchi Y. Cocktail-Dosing Microdialysis Study to Simultaneously Assess Delivery of Multiple Organic-Cationic Drugs to the Brain. J Pharm Sci. 2016;105(2):935–40.

52. Tunblad K, Jonsson EN, Hammarlund-udenaes M. Morphine Blood-Brain Barrier Transport Is Influenced by Probenecid Co-Administration. 2003;20(4):618–23.

53. Letrent SP, Polli JW, Humphreys JE, Pollack GM, Brouwer KR, Brouwer KLR. P-glycoprotein-mediated transport of morphine in brain capillary endothelial cells. Biochem Pharmacol. 1999;58(6):951–7.

54. Groenendaal D, Freijer J, de Mik D, Bouw MR, Danhof M, de Lange ECM. Population pharmacokinetic modelling of non-linear brain distribution of morphine: influence of active saturable influx and P-glycoprotein mediated efflux. Br J Pharmacol. 2007;151(5):701–12.

55. Wandel C, Kim R, Wood M, Wood A. Interaction of morphine, fentanyl, sufentanil, alfentanil, and loperamide with the efflux drug transporter P-glycoprotein. Anesthesiology. 2002;96(4):913–20.

56. Aday S, Cecchelli R, Dehouck MP, Ferreira L. Stem Cell-Based Human Blood-Brain Barrier Models for Drug Discovery and Delivery. Trends Biotechnol. 2016;34(5):382–93.

57. Feng B, Mills JB, Davidson RE, Mireles RJ, Janiszewski JS, Troutman MD, et al. In vitro P-glycoprotein assays to predict the in vivo interactions of P-glycoprotein with drugs in the central nervous system. Drug Metab Dispos. 2008;36(2):268–75.

58. Potschka H, Löscher W. In vivo evidence for P-glycoprotein-mediated transport of phenytoin at the blood-brain barrier of rats. Epilepsia. 2001;42(10):1231–40.

59. Potschka H, Löscher W. Multidrug resistance-associated protein is involved in the regulation of extracellular levels of phenytoin in the brain. Neuroreport. 2001;12(11):2387–9.

60. Dickens D, Yusof SR, Abbott NJ, Weksler B, Romero IA, Couraud PO, et al. A Multi-System Approach Assessing the Interaction of Anticonvulsants with P-gp. PLoS One. 2013;8(5).

61. Zhang C, Kwan P, Zuo Z, Baum L. In vitro concentration dependent transport of phenytoin and phenobarbital, but not ethosuximide, by human P-glycoprotein. Life Sci. 2010;86(23–24):899–905.

62. Luna-Tortós C, Fedrowitz M, Löscher W. Evaluation of transport of common antiepileptic drugs by human multidrug resistance-associated proteins (MRP1, 2 and 5) that are overexpressed in pharmacoresistant epilepsy. Neuropharmacology. 2010;58(7):1019–32.

63. Baltes S, Gastens AM, Fedrowitz M, Potschka H, Kaever V, Löscher W. Differences in the transport of the antiepileptic drugs phenytoin, levetiracetam and carbamazepine by human and mouse P-glycoprotein. Neuropharmacology. 2007;52(2):333–46.

64. Li M, Yuan H, Li N, Song G, Zheng Y, Baratta M, et al. Identification of interspecies difference in efflux transporters of hepatocytes from dog, rat, monkey and human. Eur J Pharm Sci. 2008;35(1–2):114–26.

65. Greve MW, Zink BJ. Pathophysiology of traumatic brain injury. Mt Sinai J Med. 2009;76(2):97–104.

66. Chodobski A, Zink BJ, Szmydynger-Chodobska J. Blood-Brain Barrier Pathophysiology in Traumatic Brain Injury. Transl Stroke Res. 2011;2(4):492–516.

67. Pop V, Sorensen DW, Kamper JE, Ajao DO, Murphy MP, Head E, et al. Early brain injury alters the blood-brain barrier phenotype in parallel with b-amyloid and cognitive changes in adulthood. J Cereb Blood Flow Metab. 2013;33:205–14.

68. Appel S, Duke ES, Martinez AR, Khan OI, Dustin IM, Reeves-Tyer P, et al. Cerebral blood flow and fMRI BOLD auditory language activation in temporal lobe epilepsy. Epilepsia. 2012;53(4):631–8.

69. Bednarczyk J, Lukasiuk K. Tight junctions in neurological diseases. Acta Neurobiol Exp. 2011;71(4):393–408.

70. Lazarowski A, Czornyj L, Lubienieki F, Girardi E, Vazquez S, D'Giano C. ABC transporters during epilepsy and mechanisms underlying multidrug resistance in refractory epilepsy. Epilepsia. 2007;48:140–9.

71. Löscher W, Potschka H. Role of multidrug transporters in pharmacoresistance to antiepileptic drugs. J Pharmacol Exp Ther. 2002;301(1):7–14.

72. Ball K, Bouzom F, Scherrmann J-M, Walther B, Declèves X. Development of a physiologically based pharmacokinetic model for the rat central nervous system and determination of an in vitro-in vivo scaling methodology for the blood-brain barrier permeability of two transporter substrates, morphine and oxycodone. J Pharm Sci. 2012;101(11):4277–92.

73. Loryan I, Sinha V, Mackie C, van Peer A, Drinkenburg WH, Vermeulen A, et al. Molecular properties determining unbound intracellular and extracellular brain exposure of CNS drug candidates. Mol Pharm. 2015;12(2):520–32.

74. Chen H, Winiwarter S, Fridén M, Antonsson M, Engkvist O. In silico prediction of unbound brain-to-plasma concentration ratio using machine learning algorithms. J Mol Graph Model. 2011;29(8):985–95.

75. de Witte WEA, Danhof M, van der Graaf PH, de Lange ECM. In vivo Target Residence Time and Kinetic Selectivity: The Association Rate Constant as Determinant. Trends Pharmacol Sci. 2016;37(10):831–42.

76. Ohtsuki S, Ikeda C, Uchida Y, Sakamoto Y, Miller F, Glacial F, et al. Quantitative targeted absolute proteomic analysis of transporters, receptors and junction proteins for validation of human cerebral microvascular endothelial cell line hCMEC/D3 as a human blood-brain barrier model. Mol Pharm. 2013;10(1):289–96.

77. Avdeef A, Nielsen PE, Tsinman O. PAMPA - A drug absorption in vitro model: 11. Matching the in vivo unstirred water layer thickness by individual-well stirring in microtitre plates. Eur J Pharm Sci. 2004;22(5):365–74.

78. Grumetto L, Russo G, Barbato F. Immobilized Artificial Membrane HPLC Derived Parameters vs PAMPA-BBB Data in Estimating in Situ Measured Blood-Brain Barrier Permeation of Drugs. Mol Pharm. 2016;13(8):2808–16.

79. Berezhkovskiy LM. Volume of distribution at steady state for a linear pharmacokinetic system with peripheral elimination. J Pharm Sci. 2004;93(6):1628–40.

80. Poulin P, Theil F-P. Prediction of pharmacokinetics prior to in vivo studies. II. Generic physiologically based pharmacokinetic models of drug disposition. J Pharm Sci. 2002;91(5):1358–70.

81. Aanerud J, Borghammer P, Chakravarty MM, Vang K, Rodell AB, Jónsdottir KY, et al. Brain energy metabolism and blood flow differences in healthy aging. J Cereb Blood Flow Metab. 2012;32(7):1177–87.

82. Serot JM, Béné MC, Foliguet B, Faure GC. Altered choroid plexus basement membrane and epithelium in late-onset Alzheimer's disease: An ultrastructural study. Ann N Y Acad Sci. 1997;826:507–9.

83. Shimada A, Hasegawa-Ishii S. Senescence-accelerated Mice (SAMs) as a Model for Brain Aging and Immunosenescence. Aging Dis. 2011;2(5):414–35.

84. Silverberg GD, Miller MC, Messier AA, Majmudar S, Machan JT, Donahue JE, et al. Amyloid deposition and influx transporter expression at the blood-brain barrier increase in normal aging. J Neuropathol Exp Neurol. 2010;69(1):98–108.

85. Palmer JC, Baig S, Kehoe PG, Love S. Endothelin-converting enzyme-2 is increased in Alzheimer's disease and up-regulated by Abeta. Am J Pathol. 2009;175(1):262–70.

86. Bowman G, Quinn J. Alzheimer's disease and the blood–brain barrier: past, present and future. Aging health. 2008;4(1):47–57.

87. Cipolla MJ, Sweet JG, Chan S-L. Cerebral vascular adaptation to pregnancy and its role in the neurological complications of eclampsia. J Appl Physiol. 2011;110(2):329–39.

88. Dutheil F, Jacob A, Dauchy S, Beaune P, Scherrmann J-M, Declèves X, et al. ABC transporters and cytochromes P450 in the human central nervous system: influence on brain pharmacokinetics and contribution to neurodegenerative disorders. Expert Opin Drug Metab Toxicol. 2010;6(10):1161–74.

89. Hsu JL, Jung TP, Hsu CY, Hsu WC, Chen YK, Duann JR, et al. Regional CBF changes in Parkinson's disease: A correlation with motor dysfunction. Eur J Nucl Med Mol Imaging. 2007;34(9):1458–66.

90. van Vliet EA, Araújo SDC, Redeker S, van Schaik R, Aronica E, Gorter JA. Blood-brain barrier leakage may lead to progression of temporal lobe epilepsy. Brain. 2007;130(2):521–34.

91. Ingrisch M, Sourbron S, Morhard D, Ertl-Wagner B, Kümpfel T, Hohlfeld R, et al. Quantification of Perfusion and Permeability in Multiple Sclerosis. Invest Radiol. 2012;47(4):252–8.

92. Weiss N, Miller F, Cazaubon S, Couraud PO. The blood-brain barrier in brain homeostasis and neurological diseases. Biochim Biophys Acta. 2009;1788(4):842–57.

SUPPLEMENTARY MATERIAL

S1. Calculation for the drug-specific parameters in the model.

The drug-specific parameters in the model were calculated using the following equations.

Aqueous diffusivity coefficient. The aqueous diffusivity coefficient was calculated using the molecular weight of each compound with the following equation (77).

$$\log Daq = -4.113 - 0.4609 \times \log MW \quad (1)$$

where Daq is the aqueous diffusivity coefficient (in cm^2/s) and MW is the molecular weight (in g/mol).

Permeability. Transmembrane permeability was calculated using the log P of each compound with the following equation (78).

$$\log P_0^{transcellular} = 0.939 \times \log P - 6.210 \quad (2)$$

where $P_0^{transcellular}$ is the transmembrane permeability (in cm/s), log P is the *n*-octanol lipophilicity value.

Active transport. The impact of the net effect of active transporters on the drug exchange at the BBB and BCSFB was incorporated into the model using asymmetry factors (AFin1-3 and AFout1-3). The AFs were calculated from $Kp,uu,brain_{ECF}$, Kp,uu,CSF_{LV} (unbound CSF_{LV}-to-plasma concentration ratio) and Kp,uu,CSF_{CM} (unbound CSF_{CM}-to-plasma concentration ratio), such that they produced the same Kp,uu values within the PBPK model at the steady state. The AFs were therefore dependent on both the Kp,uu values and the structure and parameters of the PBPK model. If the Kp,uu values were larger than 1 (i.e. net active influx), then AFin1, AFin2 and AFin3 were derived from $Kp,uu,brain_{ECF}$, Kp,uu,CSF_{LV} and Kp,uu,CSF_{CM}, respectively, while AFout1-3 were fixed to 1. If the Kp,uu values were smaller than 1 (i.e. net active efflux), then AFout1, AFout2 and AFout3 were derived from $Kp,uu,brain_{ECF}$, Kp,uu,CSF_{LV} and Kp,uu,CSF_{CM}, respectively, while AFin1-3 were fixed to 1. In the analysis, $Kp,uu,brain_{ECF}$, Kp,uu,CSF_{LV} and Kp,uu,CSF_{CM} were derived from previous *in vivo* animal experiments (15). The steady state differential equations in the PBPK model were solved using the Maxima Computer Algebra System (http://maxima.sourceforge.net) to obtain algebraic solutions for calculating AFs from the Kp,uu values.

S2. Calculation for the parameters using the system-specific and drug-specific parameters.

The parameters in the model were calculated using the following equations.

Passive diffusion across the brain barriers. Passive diffusion clearance at the BBB and BCSFB (Q_{BBB} and $Q_{BCSFB,}$ respectively) was obtained from a combination of paracellular and transcellular diffusion, Qp and Qt, respectively (Eq.3).

$$Q_{BBB/BCSFB}(mL/min) = Qp_{BBB/BCSFB} + Qt_{BBB/BCSFB} \quad (3)$$

where $Q_{BBB/BCSFB}$ represents the passive diffusion clearance at the BBB/BCSFB, $Qp_{BBB/BCSFB}$ represents the paracellular diffusion clearance at the BBB/BCSFB, and $Qt_{BBB/BCSFB}$ represents the transcellular diffusion clearance at the BBB/BCSFB.

The paracellular diffusion clearance was calculated with the aqueous diffusivity coefficient (Daq), $Width_{BBB/BCSFB}$ and SA_{BBBp} or SA_{BCSFBp} using equation 4.

$$Qp_{BBB/BCSFB}(mL/min) = \frac{Daq}{Width_{BBB/BCSFB}} \times SA_{BBBp/BCSFBp} \quad (4)$$

The transcellular diffusion clearance was calculated with the transmembrane permeability and SA_{BBBt} or SA_{BCSFBt} using equation 5.

$$Qt_{BBB/BCSFB}(mL/min) = \frac{1}{2} * P_0^{\,transcellular} \times SA_{BBBt/BCSFBt} \quad (5)$$

where the factor 1/2 is the correction factor for passage over two membranes instead of one membrane in transcellular passage.

Active transport across the brain barriers. To take into account the net effect of the active transporters at the BBB and BCSFB, AFs were added on $Qt_{BBB/BCSFB}$ (Eq.6 and 7).

$$Q_{BBB/BCSFB\_in}(mL/min) = Qp_{BBB/BCSFB} + Qt_{BBB/BCSFB} * AFin \quad (6)$$

$$Q_{BBB/BCSFB\_out\_withoutPHF}(mL/min) = Qp_{BBB/BCSFB} + Qt_{BBB/BCSFB} * AFout \quad (7)$$

where $Q_{BBB/BCSFB\_in}$ represents the drug transport clearance from $brain_{MV}$ to $brain_{ECF}$/CSFs, and $Q_{BBB/BCSFB\_out\_withoutPHF}$ represents the drug transport clearance from $brain_{ECF}$/CSFs to $brain_{MV}$ without taking into account the pH-dependent kinetics (to be taken into account separately; see below).

Cellular and subcellular distribution. Passive diffusion at the BCM (Q_{BCM}) and at the lysosomal membrane (Q_{LYSO}) was described with the transmembrane permeability together with SA_{BCM} or SA_{LYSO}, respectively (Eq.8 and 9).

$$Q_{BCM}(mL/min) = {P_0}^{transcellular} \times SA_{BCM} \quad (8)$$

$$Q_{LYSO}(mL/min) = {P_0}^{transcellular} \times SA_{LYSO} \quad (9)$$

where Q_{BCM} represents the passive diffusion clearance at the BCM, and Q_{LYSO} represents the passive diffusion clearance at the lysosomal membrane.

pH-dependent partitioning. We considered the differences in pH in plasma (pH 7.4) and in relevant CNS compartments, namely $brain_{ECF}$ (pH_{ECF} 7.3), CSF (pH_{CSF} 7.3), $brain_{ICF}$ (pH_{ICF} 7.0), and lysosomes (pH_{lyso} 5.0) (Friden, 2011). The impact of pH differences on the passive diffusion clearance from $brain_{ECF}$ to $brain_{MV}$ (PHF1), from CSF_{LV} to $brain_{MV}$ (PHF2), from CSF_{TFV} to $brain_{MV}$ (PHF3), from $brain_{ECF}$ to $brain_{ICF}$ (PHF4), from $brain_{ICF}$ to $brain_{ECF}$ (PHF5), from $brain_{ICF}$ to lysosomes (PHF6), and from lysosomes to $brain_{ICF}$ (PHF7) were described by pH-dependent factors, which were defined as the ratio of the un-ionized fraction of each compound at the pH in a particular compartment and the un-ionized fraction in plasma. The PHFs were calculated from the pKa of each compound and the pH of a particular compartment. The equations are developed using the classical Henderson-Hasselbalch equation (Henderson, 1908 and Henderson, 1908), and are based on the assumption that there is no active transport.

$$PHF_{base}1 = PHF_{base}4 = \frac{10^{pKa-7.4}+1}{10^{pKa-pH_{ECF}}+1} \quad (10)$$

$$PHF_{base}2 = PHF_{base}3 = \frac{10^{pKa-7.4}+1}{10^{pKa-pH_{CSF}}+1} \quad (11)$$

$$PHF_{base}5 = PHF_{base}6 = \frac{10^{pKa-7.4}+1}{10^{pKa-pH_{ICF}}+1} \quad (12)$$

$$PHF_{base}7 = \frac{10^{pKa-7.4}+1}{10^{pKa-pH_{LYSO}}+1} \quad (13)$$

$$PHF_{acid}1 = PHF_{acid}4 = \frac{10^{7.4-pKa}+1}{10^{pH_{ECF}-pKa}+1} \quad (14)$$

$$PHF_{acid}2 = PHF_{acid}3 = \frac{10^{7.4-pKa}+1}{10^{pH_{CSF}-pKa}+1} \quad (15)$$

$$PHF_{acid}5 = PHF_{acid}6 = \frac{10^{7.4-pKa}+1}{10^{pH_{ICF}-pKa}+1} \quad (16)$$

$$PHF_{acid}7 = \frac{10^{7.4-pKa}+1}{10^{pH_{LYSO}-pKa}+1} \quad (17)$$

where PHF_{base}1-7 are PHF1-7 for basic compounds, PHF_{acid}1-7 are PHF1-7 for acidic compounds, and 7.4 is the pH in the plasma compartment.

The impact of pH differences on the drug distribution among $brain_{ECF}$, CSF, $brain_{ICF}$ and lysosomes was added on Q_{BCM} and Q_{LYSO} using PHFs with the following equations 18-24, based on the assumption that the transport clearance is proportional to the un-ionized fraction of each compound.

$$Q_{BBB\_out}(mL/min) = Q_{BBB\_out\_withoutPHF} \times PHF1 \quad (18)$$

$$Q_{BCSFB1\_out}(mL/min) = Q_{BCSFB\_withoutPHF} \times PHF2 \quad (19)$$

$$Q_{BCSFB2\_out}(mL/min) = Q_{BCSFB\_withoutPHF} \times PHF3 \quad (20)$$

$$Q_{BCM\_in}(mL/min) = Q_{BCM} \times PHF4 \quad (21)$$

$$Q_{BCM_{out}}(mL/min) = Q_{BCM} \times PHF5 \quad (22)$$

$$Q_{LYSO\_in}(mL/min) = Q_{LYSO} \times PHF6 \quad (23)$$

$$Q_{LYSO\_out}(mL/min) = Q_{LYSO} \times PHF7 \quad (24)$$

where Q_{BBB_out} represents the drug transport clearance from $brain_{ECF}$ to $brain_{MV}$, Q_{BCSFB1_out} represents the drug transport clearance from CSF_{LV} to $brain_{MV}$, Q_{BCSFB2_out} represents the drug transport clearance from CSF_{TFV} to $brain_{MV}$, Q_{BCM_in} represents the drug transport clearance from $brain_{ECF}$ to $brain_{ICF}$, and Q_{BCM_out} represents the drug transport clearance from $brain_{ICF}$ to $brain_{ECF}$. Q_{LYSO_in} represents the drug transport clearance from $brain_{ICF}$ to lysosomes, and Q_{BCM_out} represents the drug transport clearance from lysosomes to $brain_{ICF}$.

Drug binding. Drug binding to brain tissue components was taken into account in the model using a binding factor (BF) under the assumption that drug binding to the tissue happens instantly. The BF was calculated from Kp (total brain-to-plasma concentration ratio) by solving the BF that results in the same Kp value in the model, using the Maxima program as described above (**Supplementary Material S1**). The Kp for each compound was calculated using the compounds' log P, the composition of brain tissue and plasma, fu,p (free fraction in plasma) and fu,b (free fraction in brain) with the following equation (79).

$$Kp = \frac{[10^{\log P} \times (Vnlb + 0.3 \times Vphb) + 0.7 \times Vphb + Vwb/fu,b]}{[10^{\log P} \times (Vnlp + 0.3 \times Vphp)] + 0.7 \times Vphp + Vwp/fu,p]} \quad (25)$$

where Vnlb, Vphb, Vwb, Vnlp, Vphp, and Vwp represent the rat volume fractions of brain neutral lipids (0.0392), brain phospholipids (0.0533), brain water (0.788), plasma neutral lipids (0.00147), plasma phospholipids (0.00083), and plasma water (0.96), respectively (80).

S3. Calculation for the active transport component of the overall permeability from *in vitro* data.

The asymmetry factors (AFs) can be derived from *In vitro* data such as efflux ratio data and cell uptake kinetics data (72).

Efflux ratio data. AFs can be derived from the information of apparent permeability (P_{app}) from apical to basolateral ($P_{app,A:B}$) and basolateral to apical ($P_{app,B:A}$), or the information of efflux ratio(ER). The active transport component of the overall permeability can be derived using the following equation (in this case, the active transporters mediate a net efflux of the drug).

$$CL_{eff,active} = \left(P_{app,B:A} - P_{app,A:B}\right) * SA_{BBB} * \text{ scaling factor} \quad (26)$$

$$ER_{eff,active} = \left(P_{app,B:A}/P_{app,A:B}\right) \quad (27)$$

where the scaling factor is used to convert values obtained from *in vitro* experiments to *in vivo* BBB values.

Cell uptake kinetics data. AFs can be derived from the information of Vmax and Km. The active transport component of the overall permeability can be derived using the following equation (in this case, the active transporters mediate a net influx of the drug).

$$CL_{uptake} = \left(\frac{Km}{Vmax + C_{u,BM}}\right) *\cdot \text{ the milligrams of protein per gram of brain} * \text{brain weight} \quad (28)$$

$$CL_{inf,active} = \left(CL_{uptake} - Ppassive * SA_{BBB} * \left(1 - \frac{C_{u,BM}}{C_{u,Plasma}}\right)\right) * \text{ scaling factor} \quad (29)$$

where $C_{u,BM}$ is free dug concentration in brain microvascular compartment, $C_{u,plasma}$ is free dug concentration in plasma compartment, Ppassive is passive permeability.

In the PBPK model, $CL_{eff,active}$, $ER_{eff,active}$, $CL_{inf,active}$ and $ER_{inf,active}$ can be derived using the following equation :

$$CL_{eff,active} = Qt_{BBB} * (PHF1 * AFout1 - 1) + Qp_{BBB} * (PHF1 - 1) \quad (30)$$

$$ER_{eff,active} = \frac{(Qt_{BBB} * AFout1 + Qp_{BBB}) * PHF1}{(Qt_{BBB} + Qp_{BBB})} \quad (31)$$

$$CL_{inf,active} = Qt_{BBB} * (AFin1 - PHF1) + Qp_{BBB} * (1 - PHF1) \quad (32)$$

$$ER_{inf,active} = \frac{(Qt_{BBB} + Qp_{BBB}) * PHF1}{(Qt_{BBB} * AFin1 + Qp_{BBB})} \quad (33)$$

where Qt_{BBB} is the transcellular diffusion rate at the BBB, Qp_{BBB} is the paracellular diffusion rate at the BBB.

Using equations 26 and 30, for example, AFout1 can be calculated from *in vitro* data.

SUPPLEMENTARY TABLES

TABLE SI. Impact of pathophysiological change on the system-specific parameters of the CNS

Pathophysiological condition	cerebral blood flow (CBF)	BBB characteristics	BCSFB characteristics	$brain_{ECF}$ bulk flow	CSF flow	Active transporters
	CBF	Paracellular diffusion	Paracellular and transcellular diffusion	Drug dispersion	Drug dispersion	AFs
Aging	decrease of the regional CBF (81)		thinner of the height of CP epithelial cells and thicker of the choroid plexus (CP) epithelial basement (82)		decrease in CSF production, increase in CSF outflow resistance (83)	loss of the function of LRP-1 and P-gp (84)
Traumatic injury	CBF reduced by 50% (65)	increase of the paracellular permeability due to the disruption of the tight junction complexes and the integrity of the basement membranes (66)				increase of pinocytotic vesicle transport across the BBB (66), decrease of the expression of P-gp (67)
Epilepsy	regional decrease of the CBF (68)	increase of the paracellular permeability due to the opening of tight junctions decrease in some tight junction proteins (e.g., occluding, ZO-1) and increase of the pinocytosis (69)				increase of the expression of P-gp and MRPs (70,71)
Alzheimer's disease (AD)	regional decrease of the CBF (85)	increase of permeability due to the abnormal opening of tight junctions (86)	thinner of the height of CP epithelial cells and thicker of the CP epithelial basement (82)	blockade of $brain_{ECF}$ flow (87)	decrease in CSF production, CSF turnover and increase in CSF volume (81)	decrease of ABCB1 (P-gp) and upregulation of ABCG2 (88)
Parkinson's disease (PD)	increase/decrease of the CBF depending on the brain region and the state of the disease (89)	increase of the paracellular permeability due to the decrease of some tight junction proteins (e.g., occluding, ZO-1) (90)				
Multiple sclerosis (MS)	increase of the CBF (91)	increase of the paracellular permeability due to the opening of tight junctions and decrease of some tight junction proteins (e.g., occluding, ZO-1, VE-cadherin) (92)				decrease of the expression of P-gp (91)

TABLE SII. Plasma PK parameter values

		Parameter estimates (RSE, %)				
		Acetaminophen		Oxycodone	Morphine	Phenytoin
		Study1 and Study2	Study 3	Study 1	Study 1 and Study 2	Study 1
CL_{PL}	mL/min	495	562 (20.1)	1030 (17.9)	3070 (15.8)	802 (65.6)
Q_{PL_PER1}	mL/min	NA	2060 (31.1)	7270 (52.1)	3030 (0.60)	7690 (12.3)
V_{PL}	mL	108000	9880 (41.1)	166000 (31.0)	16000 (35.3)	105000 (35.8)
V_{PER1}	mL	NA	51900 (18.3)	147000 (24.7)	95400 (2.50)	2000000 (5.00)
inter individual variability [a]						
ω_CL_{PL}	%	NA	49.0 (30.2)	34.1 (30.4)	27.1 (19.9)	107.7 (44.8)
$\omega\_Q_{PL\_PER1}$	%	NA	NA	NA	NA	21.1 (18.8)
ω_V_{PL}	%	NA	NA	47.2 (41.9)	59.6 (20.0)	81.0 (26.3)
ω_V_{PER1}	%	NA	23.5 (22.5)	NA	NA	NA
residual error [b]						
σ_plasma proportional	%	23.9	25.0 (8.20)	15.0 (23.4)	9.60 (22.9)	8.00 (30.5)
Ref			(15)		(15)	

CL_{PL}; clearance from the central compartment, Q_{PL_PER1}; inter-compartmental clearance between the central compartment and the peripheral compartment 1, V_{PL}; distribution volume of the central compartment, V_{PER1}; distribution volume of the peripheral compartment 1,RSE; relative standard error.

a) $\theta_i=\theta \times e^{(\eta_i)}$, where θ_i represents the parameters of the *i*th subject, θ represents the population mean value of the parameter, η_i is the random effect of the *i*th subject under the assumption of a normal distribution with a mean value of 0 and variance of ω^2.

b) $C_{ij}=Y_{IPRED,ij} \times (1+\varepsilon_{ij})$, where C_{ij} represents the *j*th observed concentration of the *i*th subject, $Y_{IPRED,ij}$ represents the *j*th individual prediction of the *i*th subject, and ε_{ij} is the random effect of the *j*th observed concentration of the *i*th subject under the assumption of a normal distribution with a mean value of 0 and variance of σ^2.